

Resonance enhanced multiphoton ionisation probing of H atoms in a hot filament chemical vapour deposition reactor

Stephen A. Redman, Charissa Chung, Keith N. Rosser and Michael N. R. Ashfold*

School of Chemistry, University of Bristol, Bristol, UK BS8 1TS. E-mail: mike.ashfold@bris.ac.uk

Received 7th December 1998, Accepted 19th January 1999

We demonstrate some of the merits and limitations of using multiphoton ionisation (MPI) spectroscopy, resonance enhanced at the two photon energy by the $2s^1;^2S_{1/2}$ state, to detect H atoms within a hot filament reactor used for diamond chemical vapour deposition (CVD). Subsequent analysis of the Doppler broadened lineshapes obtained in this way allows determination of spatially resolved, relative H atom number densities and gas temperatures. The effects of H_2 pressure and flow rate, filament temperature and radial distance from the filament on the relative H atom number densities and the gas temperature profiles have each been investigated for the case of pure H_2 and, in some cases, in the presence of added CH_4 . The present findings complement and extend previous measurements obtained using alternative *in situ* detection methods, and are generally consistent with current models of the gas phase chemistry prevailing in low power diamond CVD reactors. They also serve to refine the role of the hot filament in the H atom production process, and to illustrate continuing ambiguities regarding the way in which the local relative H atom number densities vary with filament temperature, with the presence of trace quantities of added hydrocarbon, and the interpretation of these dependencies.

Introduction

The promise of synthesised diamond films for a wide range of applications¹ ensures continued effort towards understanding the precise nature of the chemistry that underlies the chemical vapour deposition (CVD) of diamond. Macroscopic study and intuition have already gone far to make the growth of diamond from gases a useful technology, but much of the detail remains a subject of active discussion.^{2–5} A wealth of experimental data pertaining to the deposition of diamond has been collected over recent years, and it is now recognised that a comparison of intelligent modelling to this data is likely to shed most light on what is a very complicated process.

Typically, CVD diamond is grown from a dilute ($\sim 1\%$) mixture of a hydrocarbon in hydrogen. The central differences in the various deposition methods are the way in which the precursors are activated and how they are transported to the growth surface. However, common to nearly all methods is the production of atomic hydrogen, which is the driving force behind both the gas phase and many of the gas-surface reactions. The parent H_2 molecule may be dissociated on the surface of a heated filament (HFCVD), by electron bombardment in microwave plasma assisted reactors (MW-PACVD) or in the arc jet of a plasma torch. The resulting H atoms begin a series of abstraction reactions in the gas phase concocting a *pot pourri* of carbon containing species that result, at favourable pressures and temperatures, in the growth of polycrystalline diamond on a substrate.

Many species can result from the host of reactions facilitated by the large amounts of atomic hydrogen, and the local steady state gas phase composition and the resulting CVD diamond film qualities and growth rates are largely independent of the source hydrocarbon.^{5,6} Stable species that have been monitored include H_2 ,^{7–10} CH_4 ,^{7,10} C_2H_2 ,^{7,10} and C_2H_4 using techniques such as coherent anti-Stokes Raman spectroscopy (CARS),^{10–13} vacuum ultraviolet (VUV) absorption,⁹ mass spectrometry (MS)^{7,14–16} and infrared (IR) absorption.¹⁷

Laser techniques such as CARS are attractive in that they offer an unobtrusive, spatially localised measure both of the local gas temperature and of the concentration of the particular species being probed.

Radical chemistry governs the majority of CVD diamond growth with the methyl radical, CH_3 , being most favoured as the key growth species in low power (*e.g.* HF or MW-PACVD) reactors. This has been inferred from a number of experiments,^{18–20} including *in-situ* measurements²¹ above growing diamond films which indicated that CH_3 radicals were present at concentrations sufficient to account for the observed growth rates. In support of this conclusion, a growth mechanism developed by Harris²² and later modified by Harris and Goodwin²³ that takes CH_3 as the only growth species has been shown to be capable of simulating measured deposition rates in a number of growth environments. However, none of these studies rule out a contribution to growth from acetylene or other, more minor, C containing species. Optical diagnostics applied to the measurement of CH_3 radicals in diamond CVD environments include IR,¹⁷ UV^{24–26} and VUV²⁷ absorption spectroscopy, resonance enhanced multiphoton ionisation spectroscopy^{28,29} and, most recently, cavity ring down spectroscopy (CRDS).^{30,31} C atom concentrations were also monitored in the VUV absorption study²⁷ whilst C_2 and CH radicals have been monitored *via* their spontaneous emission, by laser induced fluorescence (LIF),^{32,33} by degenerate four wave mixing (DFWM)^{34,35} and by absorption spectroscopy.²⁴

Given the presence of reactive radical species in diamond CVD, it is necessary to consider both gas phase and gas-surface reactions for any comprehensive understanding of the growth mechanism. Models that include both gas-phase and gas-surface reactions have made significant recent advances, particularly for hot filament systems^{36–42} where the chemistries at the filament, substrate and the intermediate area can be treated by assuming them to be separable. Notable in this regard is the recent work of Mankelevich *et al.*⁴³ which

attempts to treat the full three dimensionality of the heat and species flux transfer processes in the vicinity of the hot filament and substrate. Accurate profiling of atom and radical concentrations is now all the more important for the purpose of validating these models.

The slow homogeneous recombination rate of atomic hydrogen at typical reactor pressures and temperatures is such that a super-equilibrium concentration exists in the vicinity of the substrate surface even though this is often remote from the point at which H atoms are produced.⁵ This abundance of H atoms is essential for high growth rates and high quality deposits. H atoms continuously create (by abstraction of surface terminating hydrogen atoms) and re-terminate (thereby preventing the reconstruction to non-diamond forms) the reactive sites necessary for the propagation of the lattice. H atoms also preferentially etch much of the non-diamond carbon deposited^{44–49} and their recombination on the substrate surface can be a significant contributor to substrate heating.^{50,51}

Optical techniques that have been investigated as candidates for H atom concentration profiling in diamond CVD reactors include direct absorption on the $n = 2 \leftarrow n = 1$ Lyman- α transition,²⁷ LIF measurements of the $n = 3 \rightarrow n = 2$ Balmer- α emission following $n = 3 \leftarrow n = 1$ two photon excitation,^{52–55} three photon resonance enhanced multiphoton ionisation ($3 + 1$ REMPI) via the $n = 2$ state⁵⁶ and *in situ* third harmonic generation (THG).^{12,57} All have attendant limitations. The large oscillator strength of the Lyman- α transition means that most growth environments will be optically thick at 121.6 nm, thus hampering estimates of H atom column densities by VUV absorption measurements. Childs *et al.*^{26,27} also report the presence of an overlapping C_2H_2 absorption feature at 121.6 nm. This, and near resonant absorption due to rovibrationally excited H_2 , must influence H atom concentration estimates based on THG measurements since these transitions will affect both the local bulk refractive index (and hence both the efficiency and the wavelength dependence of the THG generation process) and the transmission of any THG radiation from the focal region to the detector. Estimates of H atom concentrations based on $3 + 1$ REMPI measurements via the $n = 2$ state must also be treated with due caution because of the contributions from (off-resonant) THG that will almost inevitably occur at the pressures and temperatures used in most diamond CVD environments.

Thus we, and others, have focused on H atom detection methods involving *two* photon resonant excitation. Two choices merit consideration. The more widely used is two photon laser induced fluorescence (TALIF).^{55,58} Given available laser technology, $n = 3 \leftarrow n = 1$ two photon excitation at 205.1 nm with subsequent detection of the $n = 3 \rightarrow n = 2$ emission at 656.1 nm is the only practicable detection scheme, but its implementation is complicated by the need to separate the fluorescence from the intense luminous background inevitable in most deposition systems. Use of this short excitation wavelength also introduces the possibility of photochemical decomposition of hydrocarbon species (*e.g.* C_2H_2 and CH_3) present in the growth mixture, induced either by the 205.1 nm probe laser or the subsequent $n = 2 \rightarrow n = 1$ cascade emission⁵⁹ adding to the measured H atom concentrations. TALIF is also subject to collisional quenching,^{53,54} and careful calibration experiments are required prior to the extraction of absolute atom number densities. This paper describes the investigation and validation of H atom detection by REMPI at the longer excitation wavelength of 243.1 nm, resonant at the two photon energy with the $n = 2 \leftarrow n = 1$ transition. As such, it provides one of the first demonstrations of the use of REMPI spectroscopy to measure H atom spatial profiles and local temperatures, as a function of process conditions, in a CVD reactor. The present work serves to clarify the

role of the hot filament in H atom production. Studies quantifying the effect on the local H atom number density of a proximate CVD diamond surface, and its variation with temperature, will be described elsewhere.⁶⁰

Experimental

Fig. 1(a) shows a schematic of the CVD reactor incorporating a REMPI probe. The chamber comprises a six-way cross. Two side ports are equipped with flange mounted quartz windows to allow entry and exit of the probe laser beam, whilst a third (in the same horizontal plane) provides an observation window. The reactor part of the apparatus is designed so that it can be translated vertically by ≤ 25 mm relative to the fixed laser focus and REMPI probe to enable spatially resolved profiling of key species. This is achieved by suspending a cradle beneath a linear transfer mechanism attached to the top flange on which are located filament mounting posts, substrate heater plate and electrical feed-throughs. Attached to the mechanism is a pair of digital callipers, which permit positioning of the cradle with sub-millimetre precision. The cradle can also be rotated through any angle to allow measurements to be carried out

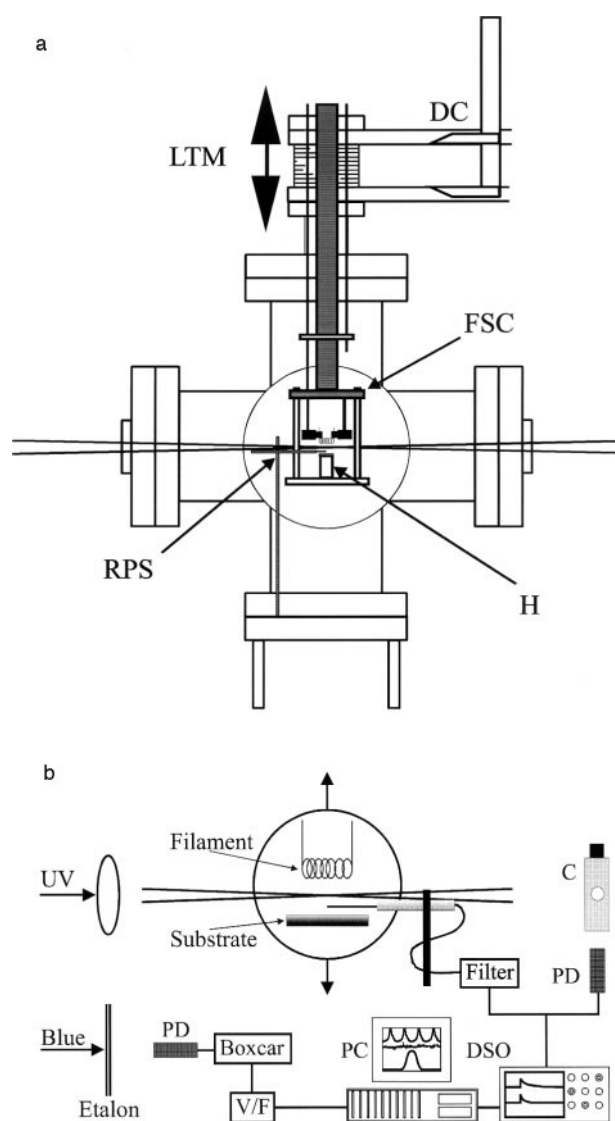


Fig. 1 (a) Schematic of the CVD reactor incorporating a REMPI probe and (b) overview of the entire experimental arrangement. Key: LTM, linear transfer mechanism, which allows vertical translation of the filament/substrate cradle by ≤ 25 mm; DC, digital callipers; RPS, REMPI probe and support; FSC, filament/substrate cradle; H, substrate heater; C, cuvette containing dilute dye solution; DSO, digital oscilloscope; PD, photodiode.

along, or perpendicular to, the filament axis. One terminal of both the substrate heater and filament is grounded. Power is supplied to the filament and substrate heater, *via* the feed-throughs, by two separate DC power supplies (Isotech IP1810H) both operating in constant current mode. The 7-turn filament is wound from 250 μm diameter tantalum or, occasionally, rhenium wire and has a coil diameter of ~ 3 mm. Typically, in pure H_2 , the filament draws 6.5 A at ~ 12.5 V, maintaining a colour temperature of $\sim 2100^\circ\text{C}$ as measured by a two-colour optical pyrometer (Land Infrared FRP12). The pyrometer controller allows the user to select a non-greyness factor to compensate for the fact that the target emissivity may be wavelength dependent in the monitored range (0.8–1.1 μm). A non-greyness factor of 1.0 was selected as a result of calibration experiments in which the filament resistance, in vacuum, was monitored as a function of measured filament temperature, T_{fil} . Comparison with tabulated values of the temperature dependent resistivity of Ta⁶¹ indicates that the emissivity does not vary significantly over this wavelength range, vindicating this choice of factor for valid temperature measurement. The substrate, when in place, is mounted on a purpose designed heated copper block, and the substrate temperature monitored by a type K thermocouple tip embedded in the top surface of this block.

Prior to any experiment, the chamber is evacuated to a base pressure of $\sim 10^{-2}$ Torr using a rotary pump (Edwards 8 Two Stage) connected to the remaining side flange. Experiments reported herein employ either pure H_2 , or $\leq 2\%$ CH_4 in H_2 , which is pre-mixed in a manifold and then fed into the reactor through a port located above the cradle assembly. Mass flow controllers (MFCs, Tylan) in series with a needle valve are used to maintain a total flow of 100 sccm at a chamber pressure of 20 Torr. Two additional MFCs are in place to facilitate future additions of trace gases. Fig. 1(b) shows the experimental layout for H atom excitation, signal collection and data processing. H atoms are detected by 2 + 1 REMPI on the $2s \leftarrow 1s$ transition using 243.1 nm radiation generated by a Nd-YAG pumped dye laser (Quanta-Ray DCR-2A plus PDL-3) operating at 10 Hz, using the dye Coumarin 480 and subsequent frequency doubling (in BBO) with a home built 'autotracker.' The UV light is separated from the dye fundamental using a Pellin-Broca prism, attenuated to energies < 100 μJ per pulse and focused into the centre of the reactor using a 20 cm focal length quartz lens. A fraction of the UV light exiting the reactor is diverted into a cuvette containing dilute Rhodamine 6G solution using a quartz beamsplitter, and the resulting fluorescence monitored by a photodiode for power-normalisation purposes. The frequency dispersion is measured by directing part of the fundamental dye laser beam through an etalon and recording interference fringes, whose separation [$1.250(4)$ cm^{-1} in the visible] had been determined previously by comparison with well documented transitions of atomic neon excited in an optogalvanic lamp.

The relative merits of detecting the photoelectrons and protons generated in the REMPI process have been explored. These are collected on a suitably biased 750 μm diameter platinum wire probe, the end of which is positioned ~ 2 mm from the laser focus so as not to be in the waist of the beam. Celi and Butler⁵⁶ used a similar probe in their fixed position REMPI experiments and the choice of platinum as a material that will not significantly alter the local gas phase composition has been vindicated.¹⁴ The shaft of the probe is shrouded in a ceramic tube, so that it may be biased with respect to the grounded reactor walls, leaving the last ~ 10 mm bare. A filter and accompanying power supply prevent the probe bias, and hence collection efficiency, changing from its nominal value due to differing thermionic emission levels at different values of d , the perpendicular distance separating the laser focal volume from the filament, whilst passing the transient REMPI current. The current requires no amplification and is fed,

along with the signal from the photodiode monitoring UV power, into a digital oscilloscope (LeCroy 9361) and thence, *via* a GPIB interface into a PC for storage and subsequent analysis. Another photodiode is used to monitor the etalon transmission in the visible; its output is fed *via* a linear gate (SRS 250) and thence to the PC.

Detection of the photoelectrons proved to be problematic.⁶² The filament was arranged with a negative potential across it in order to minimise photoelectron migration to the filament. However, the nominal probe bias (~ 13.5 V) was found to decrease as the hot filament approached the probe region—an effect attributable to the probe drawing more thermionic current. This decrease in bias altered the collection efficiency and thus precluded reliable number density measurements. Celi and Butler⁵⁶ were able to detect REMPI electrons on a grounded wire in a hot filament reactor, but these were static measurements at a constant filament distance and were thus not affected by changing background thermionic levels (though they presumably experienced more thermal electron emission at higher filament temperatures). Corat and Goodwin²⁸ detected electrons from REMPI of CH_3 radicals in a HFCVD reactor using a probe, similar to that employed here, maintained at 20 V higher than a positively biased filament. They reported that the electrical noise from thermionic emission was filtered when using this biased filament power supply, presumably (at least partly) because of thermionic entrapment caused by the positive field around the filament. They worked in a regime where electron saturation was achieved for different substrate temperatures but again made static measurements. The detection of REMPI electrons in a background of thermionic electrons is, of course, susceptible to noise associated with any variations in the filament characteristics during an experiment. Thus the use of a positively biased filament was investigated in an attempt to contain the thermionic emission. This arrangement was capable of maintaining a stable collection efficiency for filament distances $d > 4$ mm but, at smaller distances, this efficiency was reduced and the measured signal quenched, possibly by REMPI electron loss to the filament itself. Gas temperature determination *via* Doppler lineshape measurements involving this scheme remains faithful, however, provided that a constant fraction of the electrons is detected.

Thus the alternative strategy, involving collection of protons formed in the focal volume, was adopted. This required use of a negatively biased probe and a positive potential across the filament. Use of a negative bias made fixing the probe bias at any chosen value (*e.g.* -48.5 V) more facile, as little or no thermionic current is drawn. It was recognised that the positive filament polarity should induce a space-charge region in the near vicinity, as is present in valve components. To investigate the possible importance of such effects on experimental sensitivity at small d a pulsed detection scheme was implemented whereby, shortly before each laser shot, the filament power was triggered off and remained off for ~ 2 ms. The probe laser was fired ~ 0.5 ms into this period, anticipating that any charge cloud would by then have dispersed, and the H^+ time of arrival (TOA) signal collected. The pyrometer showed no discernible change in T_{fil} due to this switching. The oscilloscope trace revealed a small decrease in the probe potential for those 2 ms, consistent with the idea of escaping charges, on the back of which the proton signal was clearly evident. Use of this more elaborate switched power supply arrangement was found to have no overall effect on the measured signal and is thus no longer used. Proton collection affords substantially better signal to noise in the measurements as it is insensitive to changes in thermionic background; generation of positively charged fragments by a new filament is observed as noise but once the filament has been 'seasoned' by running for a short period of time this noise is seen to disappear.

Results and discussion

Validation of the 2 + 1 REMPI detection scheme

Unless specifically stated otherwise, all of the results reported here were obtained using pure H₂ gas input flowing at 100 sccm, maintained at 20 Torr chamber pressure, with no substrate present, and the probe laser propagating parallel to the long axis of the filament. Prior to any use of REMPI detection methods to provide quantitative estimates of the local gas temperature and relative number densities several factors need to be considered. These include: (a) Saturation of the H⁺ ion collection efficiency. Traditionally this is demonstrated by observing a plateau region in the REMPI signal *vs.* probe bias plot whilst all other parameters are held constant.^{28,63–65} For different *d* this plateau region may occur at different probe biases due to changes in the electric field gradient between filament and probe. Nonetheless, as Fig. 2 shows, it was possible to find a probe bias that satisfied the saturation requirement for all given filament distances used in the present work. The H atom REMPI signal, *S*, used in this and all other data sets displayed in this work was the total ion signal reaching the probe in a 1 ms detection window, the opening of which is coincident with the firing of the REMPI laser. Errors in the individual measurements reported in this and later figures are estimated to be comparable to, or smaller, than the plotted data points unless shown otherwise. As we show below, selecting a sufficiently wide time window to allow collection of the entire H⁺ TOA signal is a key requirement of the REMPI detection scheme. A probe bias of -48.5 V was chosen (from inspection of Fig. 2) and was used for all of the following experiments. The gradual increase in signal above the plateau region in this figure is attributed to accelerated charges causing secondary ionisation. (b) The relationship between *S* and the UV pulse energy, *E*. Fig. 3 shows the results of such measurements, in the form of a log–log plot. The deduced gradient, ~ 2.0 , implies that the REMPI signal is proportional to the square of the UV pulse energy, which suggests that, under the prevailing experimental conditions, the final one photon absorption step in the 2 + 1 REMPI process proceeds with near unit efficiency. This quadratic relationship ($S \propto E^2$) has been assumed throughout when correcting the measured ion currents for shot-to-shot variations in the UV light intensity. Deviation from the straight line at the highest values of *E* reflects the expected onset of saturation effects, and care is taken before every experiment to try to ensure that this regime is avoided. The vertical arrow in Fig. 3 indicates the normal working condition. (c) The absence of any unintentional broadening of the measured lineshapes. Fig. 4 shows represen-

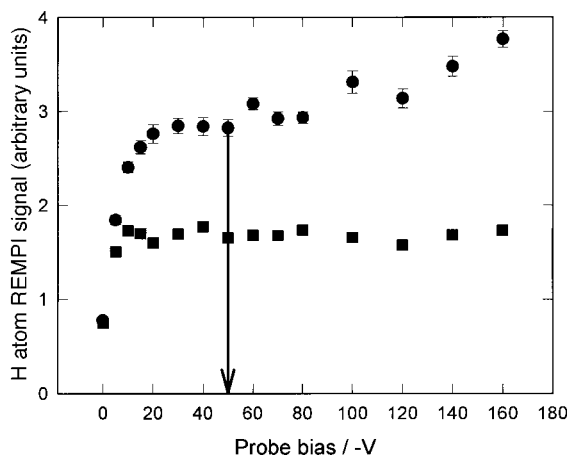


Fig. 2 Ion signal resulting from 2 + 1 REMPI at 243.1 nm measured at *d* = 2 (●) and 10 mm (■), plotted as a function of negative bias voltage. The working potential of -48.5 V lies in the plateau region of both plots.

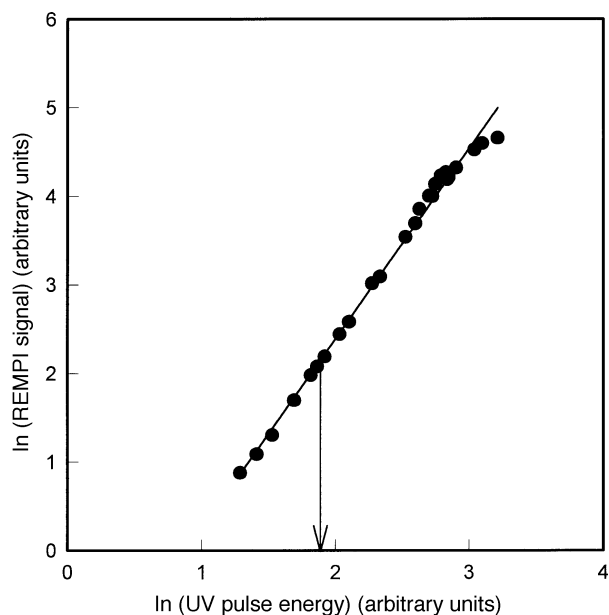


Fig. 3 Log–log plot of REMPI signal *versus* 243.1 nm laser pulse energy (as determined by monitoring the intensity of laser induced fluorescence from the cuvette of dilute Rhodamine 6G solution). The solid line represents a gradient of 2.0. ‘Normal’ operating conditions are indicated by the vertical arrow.

tative lineshapes of the 2s \leftarrow 1s two photon transition of atomic H recorded by monitoring the entire proton TOA signal reaching the probe as a function of excitation wavelength. For these two spectra the lower limb of the filament was, respectively, 0.5 and 10 mm above the laser focus and the input gas was pure H₂. Each data point is the summation of 10 laser shots and has been normalised against E^2 as described above. The solid line through the data points is the result of a least-squares fit using a Gaussian lineshape function. Clearly, such a function provides a good fit to the experimental lineshapes. The probe laser lineshape (assumed Gaussian, with a 0.07 cm⁻¹ FWHM in the UV) makes minimal contribution to the measured linewidth and, after

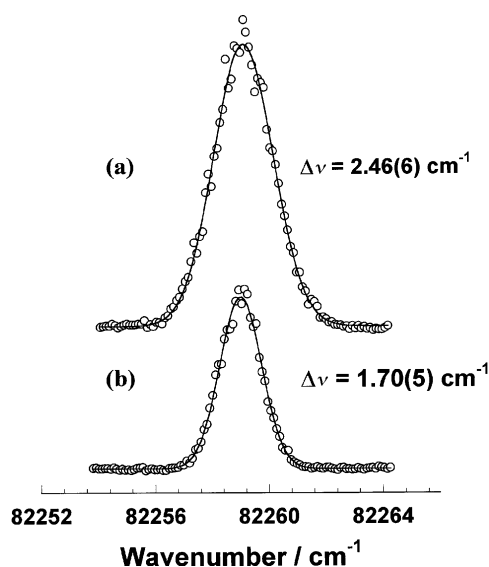


Fig. 4 Representative Doppler lineshapes of the H atom 2s \leftarrow 1s two photon transition recorded in 20 Torr of pure H₂ with the laser focus at (a) *d* = 0.5 and (b) *d* = 10 mm from the bottom of the hot coiled Ta filament held at $T_{fil} = 2375$ K. The solid curve in each case is a least squares fit to a Gaussian function, the FWHM of which (after deconvolution of the laser linewidth) yields a measure of the local temperature, whilst the areas under such lineshapes provide a measure of the relative H atom number density.

deconvoluting this contribution, it is tempting to ascribe the remaining linewidth to the effects of Doppler broadening. In such a picture Δv_D , the FWHM linewidth, provides a measure of the local translational temperature *via* the relationship:

$$\Delta v_D = \frac{v_0}{c} \sqrt{\frac{8kT \ln 2}{M}} \quad (1)$$

where v_0 is the line centre transition frequency, c the speed of light and M the mass in kg. At this juncture it is necessary to consider what else might contribute to this measured linewidth. Pressure (collisional) broadening is assumed to make an insignificant contribution under the prevailing process conditions. Unlike 3 + 1 REMPI *via* the $2p^1;^2P^o$ excited state or detection schemes involving two photon excitation to the $n = 3$ level, no significant fine-structure splittings affect the $2s \leftarrow 1s$ two photon transition. Lifetime broadening must, however, be considered. The mean fluorescence lifetime of the $H(n = 2)$ state (even allowing for collision induced l mixing) is far too long to contribute any uncertainty broadening to the measured linewidth, but absorption of (and ionisation by) a third 243.1 nm photon within the focal volume is likely whenever using a focused laser beam. This ionisation process will reduce the mean lifetime of atoms in the resonance enhancing $n = 2$ state and, in the limit of high power densities and high ionisation rates, can be expected to cause a homogeneous (Lorentzian) contribution to the measured lineshape. By working within the low power regime, where $S \propto E^2$ and the narrowest (*i.e.* large d) REMPI lineshapes are well described by a Gaussian function, we can be confident that power broadening makes negligible contribution to the measured linewidths, or to the gas temperatures derived therefrom.

Even in this low power regime, however, it was necessary to guard against one other 'saturation' effect, which is evident at the highest signal intensities (*e.g.* at small d and high filament temperatures). This saturation manifests itself most clearly through the anomalously large linewidths (and the unphysical translational temperatures that eqn. (1) would thus imply) that result. Careful examination shows that no single Gaussian will provide a comparably good fit both to the wings and the central portion of such a saturated lineshape, and that the H^+ TOA spectrum recorded at line centre is anomalously extended. All of these observations are explicable in terms of space-charge effects. These cause reduced H^+ collection efficiency and thus detection sensitivity at line centre, and a consequent overestimation of the FWHM linewidth. Given the unavoidable slight variations in beam alignment from experiment to experiment, each set of measurements was preceded by a series of checks to ensure that lineshapes were recorded at sufficiently low incident laser intensities that the measured linewidth was insensitive to the UV pulse energy, *i.e.*, that all recognised saturation effects made negligible contribution to the measured linewidths. Under these circumstances the area under the fitted Gaussian provides a measure of the relative H atom number density, $[H]$, in the focal volume. Relative mole fractions, x_H , can be calculated (assuming ideal gas behaviour) by scaling the measured relative number densities by the deduced local temperatures (or by a smooth fit to the measured temperature profile).

H atom number density as a function of H_2 pressure and flow rate

Fig. 5(b) shows plots of $[H]$ measured at $d = 1$ and $d = 5$ mm from the filament, at a constant H_2 flow rate of 100 sccm, as a function of H_2 pressure, $p(H_2)$, in the range 10.6 to 41.5 Torr. The power supplied to the filament remained almost constant throughout these measurements, but T_{fil} was observed to fall slightly with increasing $p(H_2)$. Both T_{fil} and the local gas temperatures deduced from Doppler lineshape analysis at each position and at each $p(H_2)$ are illustrated in Fig. 5(a). As this

shows, the gas temperatures measured at both d first increase and then show a gradual decrease with increasing $p(H_2)$. Such trends match well with the calculated temperature profiles of Meier *et al.*,⁵³ for a similar range of pressures, and are generally consistent with the expectation that the thermal conductivity of the gas improves with increasing $p(H_2)$. Thus the gentle increase at low pressure is attributable to improved heat transport from the filament, while the subsequent decrease at higher pressures probably reflects both the observed decrease in T_{fil} and increased heat loss to the cold reactor walls.

Fig. 5(b) shows $[H]$ to be almost invariant to $p(H_2)$ throughout the range of pressures investigated, thereby reinforcing the conclusions reached in the earlier TALIF studies,^{52,53} and from measurements of the pressure dependence of the power consumption by hot Ta and W filaments when used to dissociate H_2 .⁶⁶ All are consistent with the assumption that, at the prevailing pressures and temperatures, the dominant H atom formation mechanism is H_2 bond fission on the surface of the hot filament with kinetics that are thus zero order with respect to $p(H_2)$. The very gradual decrease in $[H]$ observed at higher $p(H_2)$ likely reflects an increasing contribution from the three body homogeneous recombination



with, in this case, $M = H_2$. Measurements using 20 Torr of H_2 feed gas and a reduced flow rate of 50 sccm yielded local gas temperatures and relative $[H]$ signals that were indistinguishable from those shown in Fig. 5. Such observations are consistent with the view that diffusion is the dominant transport mechanism in low pressure (*e.g.* HFCVD) reactors.^{37,41,50,66}

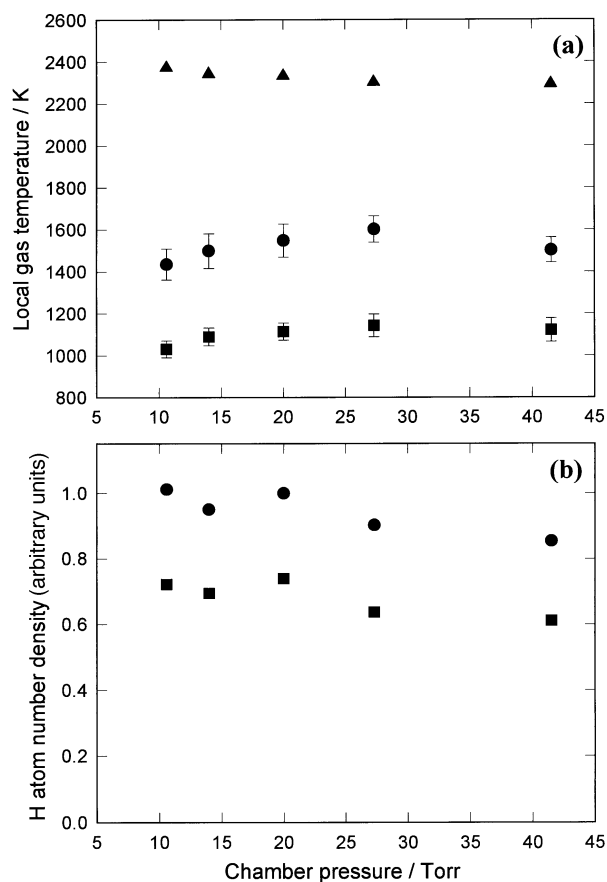


Fig. 5 (a) Translational temperatures and (b) relative number densities of H atoms deduced from analysis of the $2s \leftarrow 1s$ two photon Doppler lineshapes recorded at $d = 1$ (●) and 5 mm (■), plotted as a function of $p(H_2)$. T_{fil} (▲, by optical pyrometry) varies weakly with $p(H_2)$ as shown in (a).

Effect of filament temperature

More evidence for the pivotal role of the filament surface in H atom production in a HFCVD reactor is provided by Fig. 6, which shows how the H atom translational temperature and relative H atom number density measured at $d = 1$ mm in 20 Torr of pure H_2 vary with T_{fil} . The local gas temperature as determined from Doppler lineshape analysis increases approximately linearly with increasing T_{fil} , but even 1 mm from the filament is ~ 700 K cooler than the filament surface as measured by optical pyrometry. Temperature discontinuities of this magnitude have been reported previously,^{9,11,12,53} and accord with expectations based on the original work of Langmuir.⁶⁷ The solid line is a linear regression fit to the measured gas temperatures. $[H]$ increases approximately exponentially in the temperature range investigated. We observe very similar dependencies at $d = 4$ mm, as did Celii and Butler⁵⁶ when using 3 + 1 REMPI to monitor H atoms in an HFCVD reactor at $d = 8$ mm. T_{fil} was not raised high enough in the present work to observe any plateau of H atom production such as has been reported in previous studies of H_2 decomposition on a hot metal surface.⁶⁸

Fig. 7 shows that a van't Hoff type plot of $\ln[H]$, measured at $d = 1$ mm, versus $1/T_{\text{fil}}$ yields a straight line. The gradient of such a plot can be interpreted in terms of $-\Delta H_{\text{diss}}/R$, where ΔH_{diss} (here determined as 237 kJ mol^{-1}) is an effective enthalpy for forming one H atom by H_2 decomposition on the surface of the hot Ta filament. A significant source of uncertainty in this measurement is likely to be the absolute accuracy of the pyrometer measurement of T_{fil} ; at these temperatures a systematic error of ± 100 K would translate into a $\pm 22 \text{ kJ mol}^{-1}$ uncertainty in ΔH_{diss} . The data taken in

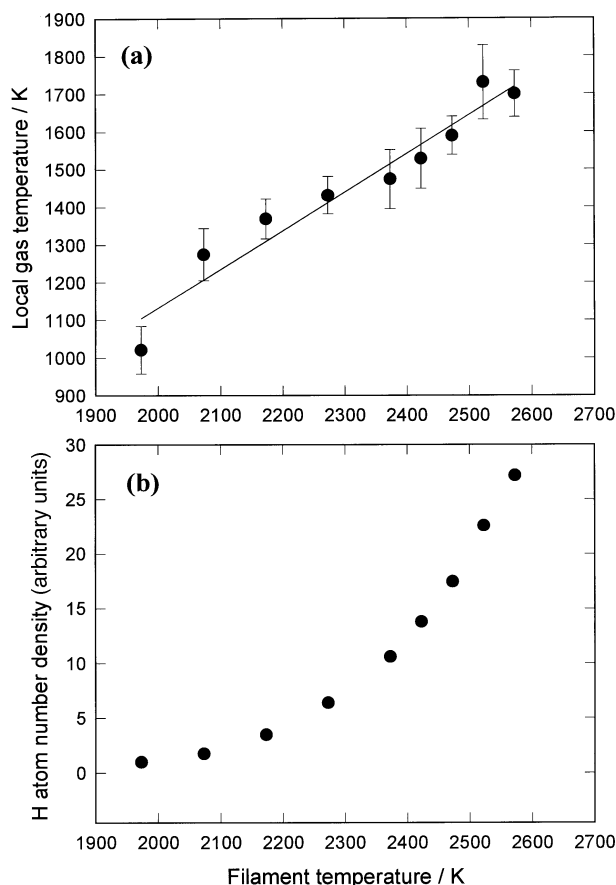


Fig. 6 (a) Translational temperatures and (b) relative number densities of H atoms deduced from analysis of the $2s \leftarrow 1s$ two photon Doppler lineshapes measured at $d = 1$ mm, plotted as a function of T_{fil} . The solid line in (a) is a linear least squares fit to the deduced temperatures.

pure H_2 at $d = 4$ mm yield a slightly steeper gradient (corresponding to $\Delta H_{\text{diss}} \sim 268 \text{ kJ mol}^{-1}$). Analogous experiments were attempted using $125 \mu\text{m}$ diameter rhenium and tungsten filaments. The former behaved similarly to Ta, yielding straight line van't Hoff type plots (at least for $T_{\text{fil}} \leq 2400$ K), the gradients of which were consistent with $\Delta H_{\text{diss}} \sim 230 \text{ kJ mol}^{-1}$. In contrast, the W filament expanded and distorted to an extent that precluded definition of a constant d as T_{fil} was increased. These ΔH_{diss} values accord well with those we obtain by plotting data from the earlier 3 + 1 REMPI measurements of Celii and Butler,⁵⁶ probing at $d = 8$ mm in 25 Torr of pure H_2 , in a similar manner, but are some 20% higher than the values deduced by Otsuka *et al.*⁶⁶ in their studies of the electrical power consumed by hot Ta and W filaments in the presence of H_2 .

How should we interpret these ΔH_{diss} values? H atom production in HFCVD reactors is visualised in terms of reversible elementary steps of the type



where reactions (3) and (−3) represent dissociative adsorption of H_2 on an active site (S^*) on the metal surface and H atom recombination on a hydrogen terminated surface site, respectively, and reactions (4) and (−4) involve desorption and adsorption of an H atom. Increasing T_{fil} will influence the local $[H]$ through its possible effect on all backward and forward reaction rates—not just by helping to overcome any energy barriers associated with the various processes as written, but also by affecting the mean lifetime of any chemisorbed species on the filament surface, the balance between non-dissociative (not shown) and dissociative adsorption (3), the fraction of surface sites that are ‘active’ (*i.e.* S^* versus SH), the local gas phase $[H]$ [which affects the extent of contributions from reaction (4)], and the local total number density. This last factor will influence the diffusion rate away from the hot filament source and the various species concentration profiles and the rates of the various gas phase reactions occurring in the immediate vicinity of its surface.

Notwithstanding this complexity, we recognise that the sum of these two reactions is simply H_2 decomposition at the surface. Fig. 7 also shows (bold solid line) the $\ln[H]$ versus

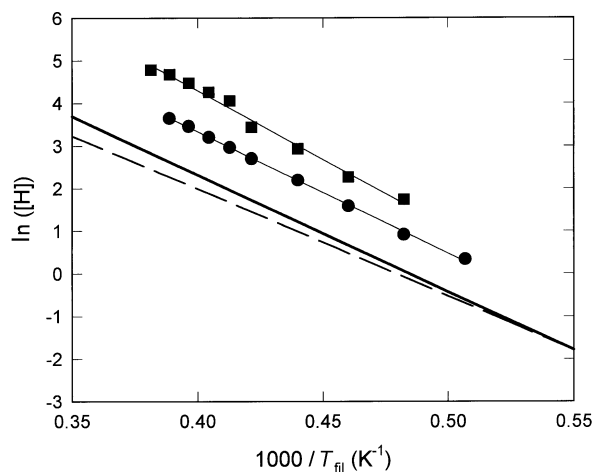
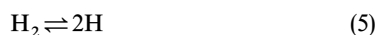


Fig. 7 Van't Hoff plot illustrating the good linear correlation between $\ln[H]$ and $1/T_{\text{fil}}$ using 20 Torr pure H_2 and measuring at $d = 1$ (●) and 4 mm (■). The two data sets are offset from one another for clarity of presentation. Interpreting the gradients in terms of $-\Delta H_{\text{diss}}/R$ yields effective dissociation enthalpies of, respectively, 237 and 268 kJ mol^{-1} . The bold solid line shows the dependence expected on the basis of the tabulated temperature dependence of K_f for reaction (5), while the dashed line shows how this would be modified if a homogeneous gas phase sample of H_2 was heated to temperatures in the same range whilst maintaining the pressure constant.

$1/T$ dependence we should expect simply on the basis of the tabulated⁶⁹ temperature dependence of the equilibrium constant, K_f , for the gas phase reaction:



and use of the relationship

$$[\text{H}] = \left(\frac{4K_f^2}{4 + K_f^2} \right)^{1/2} \quad (6)$$

The resulting gradient gives $\Delta H_{\text{diss}} = 228 \text{ kJ mol}^{-1}$. The close similarity between this and the measured dependencies in pure H_2 , taken together with the H mole fraction estimates reported elsewhere^{5,12} and the observed insensitivity of $[\text{H}]$ to $p(\text{H}_2)$, all support the view that the key role of the filament surface is to provide an efficient means by which H_2 molecules can attain T_{fil} . Of course, were it possible to heat a gas phase sample of H_2 homogeneously to the same temperature (at constant pressure) the measured $[\text{H}]$ yield should be expected to show a slightly shallower temperature dependence ($\Delta H_{\text{diss}} \sim 207 \text{ kJ mol}^{-1}$ in the temperature range of interest) because of the inverse dependence between total number density and temperature that follows if we assume ideal gas behaviour. This is shown by the dashed line in Fig. 7.

H atom number density and temperature profiles in pure H_2

Fig. 8(a) and 8(b) show, respectively, the H atom translational temperature and the relative number density profile, each plotted as a function of d . The origin ($d = 0$) in these experiments was determined by translating the filament assembly until the transmitted beam first shows obvious evidence of obstruction from the lowest part of each loop of the hot filament coil, and then zeroing the digital calliper. Two data sets are included in each figure; one obtained by collecting the entire H^+ TOA signal using the 1 ms gate, the other collecting just that fraction of the ion current arriving in a narrow (20 μs) time gate set close to the peak of the TOA signal, as illustrated in the inset to Fig. 8(a). The differences can be rationalised in terms of the temperature distribution within the gas. The REMPI probe tip and the minimum beam waist are arranged to be at the mid-point of the filament length, but the effective length of the focal region within which REMPI can occur is judged to be of the order of the filament length. Belated protons collected from the extremities of this focal volume derive from H atoms in somewhat cooler regions than the H atoms giving rise to protons collected at early TOAs, which originate from hotter regions within the laser focus, closest to the probe. This probably explains why the narrow gate data consistently yield slightly greater Doppler widths, implying higher gas temperatures than the all-incorporating gate. Additionally, we note that the H^+ TOA signal extends in time as d is increased. This is understandable since, as the filament is withdrawn, the average gas temperature in the vicinity of the laser focus decreases [Fig. 8(a)] and hence the local number density increases. As a result, the proton mean free path (calculated to be $\sim 70 \mu\text{m}$ at 1000 K if we assume a $\text{H}^+ - \text{H}_2$ collision cross-section of 0.1 nm^2) is reduced, and these ions take longer to diffuse a given distance to the probe. Clearly, any narrow time gate set on the TOA signal is unlikely to span a constant fraction of the REMPI signal and thus will not yield reliable spatial profiles. For example, the narrow 'early' gate used in obtaining the data displayed in Fig. 8 was set on the peak of the TOA signal observed for small d . As the filament was withdrawn, the peak TOA signal 'walked' out of this gate, with the result that a smaller fraction of the total signal was collected. Thus we consider it preferable to collect the *entire* TOA signal, recognising that the profiles so derived necessarily include a greater degree of averaging throughout the focal volume. In this regard REMPI probing arguably offers less spatial definition than the alternative TALIF technique, if the resulting fluorescence is imaged

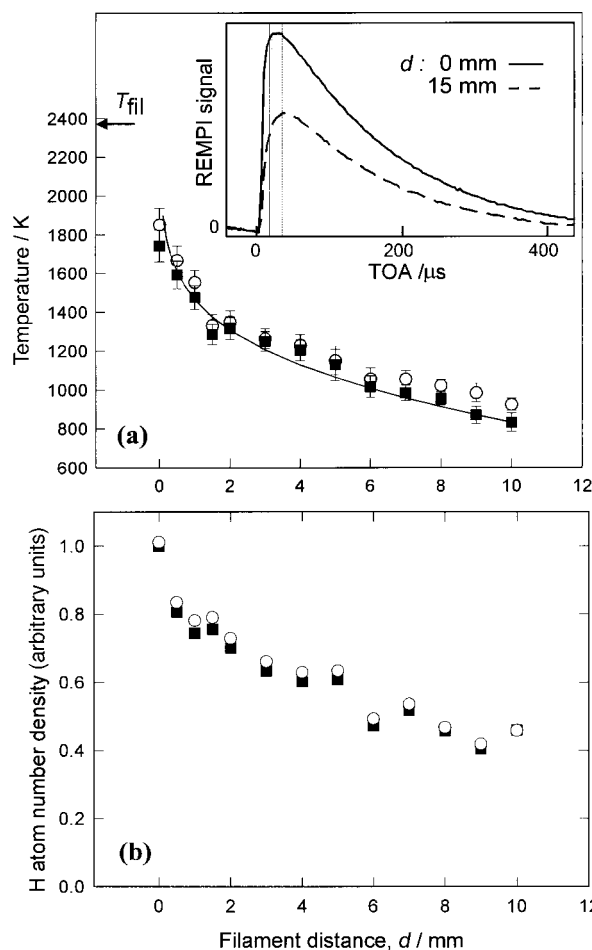


Fig. 8 Variation of (a) the local gas temperature and (b) the relative H atom number density in 20 Torr of pure H_2 with $T_{\text{fil}} = 2360 \text{ K}$, as deduced from analysis of the H atom $2s \leftarrow 1s$ two photon lineshapes, plotted as a function of d . Lineshapes were measured monitoring just that fraction of the H^+ ion TOA signal that fell within a short, early time gate [O, illustrated in the inset in (a)] and by collecting the entire TOA signal within 1 ms of the laser firing (■). The solid curve in (a) is a fit to the latter data using eqn. (7).

with well designed collection optics. Conversely, TALIF of course becomes increasingly difficult at small d given the intense background emission from the incandescent hot filament.

The solid line through the data points in Fig. 8(a) is obtained using expression (7), which is obtained from 2D diffusive calculations⁴² involving solution of the conservation equations for mass, momentum, energy and species concentration, and the assumption that conduction is the dominant heat transport mechanism:

$$T_d = T_{d=0} \{ 1 - [1 - (T_L/T_{d=0})^2] \ln(d/R_f) \ln(L/R_f) \}^{0.5} \quad (7)$$

where $T_{d=0}$ and T_L are the gas temperature very close to the filament and at a distance L from the filament, respectively, and R_f is the filament radius (125 μm). The good agreement between experiment and eqn. (7), which has been used to model the radial gas temperature profiles in other axially symmetric HFCVD reactors,^{11,52} provides further validation of the model⁴² and of the fact that H atom Doppler lineshape analysis represents a viable (and relatively straightforward) alternative to CARS as a reliable means of probing spatially localised gas temperatures in a HFCVD reactor.

Childs *et al.*²⁷ used VUV absorption at the Lyman- α wavelength to determine H atom mole fractions in a HFCVD reactor in the absence of hydrocarbon input, and inferred absolute x_{H} values from C and CH_3 density measurements

when hydrocarbon was present. Direct measurement of absorption due to atomic H in the presence of hydrocarbon was not possible in their work because of the blending of a C_2H_2 absorption feature. This study involved a reactor not dissimilar to ours, using a gas mixture of 1% CH_4 in H_2 and a straight W filament heated to 2500 K, and also involved 2D modelling of the temperature, flow, diffusion and C_1 chemistry. Fig. 9 compares the general form of their inferred x_H values (both from experiment and simulation) with relative mole fractions deduced from the present study. These were obtained by multiplying the measured $[H]$ values [Fig. 8(b)] by the smooth fit to the temperatures determined using the 1 ms time gate [Fig. 8(a)]. Despite the absence of CH_4 in the present gas mix and the differences in filament material, temperature and geometry, the two experimental data sets clearly show many similarities. The apparent divergence between experiment (shown by the individual data points) and the simulation at $d > 10$ mm is probably a consequence of a substrate, at $d = 14$ mm, in the work of Childs *et al.*²⁷ This must act as a sink for H atoms and, in the simulation, x_H was thus assumed to decrease asymptotically to zero at the substrate surface. The numerical simulation also demonstrated that the presence of a small amount of methane in the feed gas has little effect on the H atom concentration profiles, further encouraging direct comparison of the two data sets. Comparable monotonic declines in x_H versus d in HFCVD reactors have also been deduced using the recombination enthalpy technique⁷⁰ and *via* more direct TALIF⁵³ and THG¹² probing of the H atoms. All highlight the fact that efficient H atom production (by heterogeneous decomposition on the hot filament) and the lack of sink reactions ensure ‘super-equilibrium’ (*i.e.* far greater than predicted by local equilibrium thermodynamics) gas phase H atom number densities at all d .

Effect of CH_4 addition on H atom number densities

Addition of even trace amounts of CH_4 leads to carburisation of the filament and complicates the chemistry prevailing in a HFCVD reactor considerably, by introducing a wider variety of surface sites—the relative concentrations, reactivities and stabilities of each of which will exhibit their own characteristic temperature dependence—and offering new and efficient reactive loss mechanisms (both heterogeneous and homogeneous) for H atoms. Some of these complications are illustrated by the results shown in Fig. 10 and 11. The data shown in Fig. 10 were taken using a Ta filament, current limited to 6.5 A.

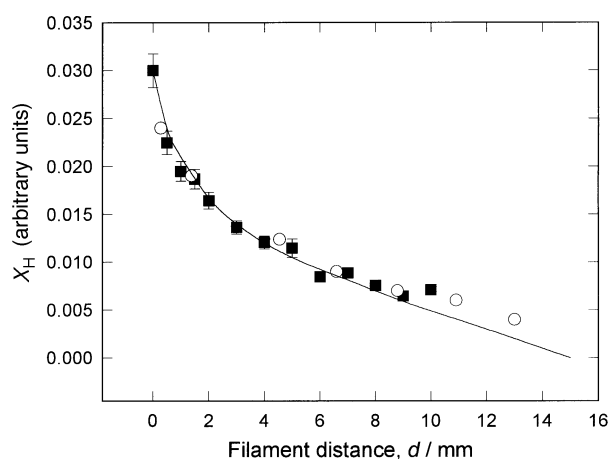


Fig. 9 Plot of x_H versus d , (■), derived from measurements of the relative H atom number density and gas temperature profiles in 20 Torr of pure H_2 with $T_{fil} = 2360$ K, as shown in Fig. 8. The measured radial dependence accords well with the previous measurements (○) and simulation (—) reported by Childs *et al.*²⁷

Under our standard conditions this resulted in $T_{fil} = 2360$ K (as measured by optical pyrometry) once the filament I – V characteristics had settled. Local gas temperatures were deduced from analysis of H atom Doppler profiles measured at $d = 0.5$ and 4.5 mm. Fig. 10 shows the time evolution of the filament and local gas temperatures after introducing a steady flow of 0.5% CH_4 . T_{fil} showed an apparent ~ 50 K decrease in the first ~ 2 min after CH_4 addition, even though the power to the filament had already increased slightly. Thereafter, the measured T_{fil} was observed to increase over the next ~ 360 min and then to decline gradually. The measured gas temperatures follow this trend closely. After $t = 2$ min, the filament resistance, and hence the voltage it drops at constant current, increased steadily—presumably due to increasing carbon dissolution in and/or carbide formation on the filament—and then decreased in parallel with the optical pyrometry measurements. This encourages the assumption that any changes in the emissivity of the filament surface upon carburisation were not invalidating our measurements of T_{fil} . The observed linearity of the plot of filament power ($I \times V$) versus the fourth power of the measured T_{fil} lends further support to this assumption in that it suggests that, apart perhaps from the very early carburisation stage, the filament emissivity does not vary sufficiently to negate expectations based on Stefan’s law. Similar behaviour was observed when adding 0.75% CH_4 , though in this case T_{fil} was observed to maximise somewhat earlier ($t \sim 160$ mins) and to decrease gradually thereafter. In both cases, we suggest that the longer term decline may reflect expulsion of carbon from the filament once some critical carbon content and/or temperature is exceeded; given such a competing process it is probable that

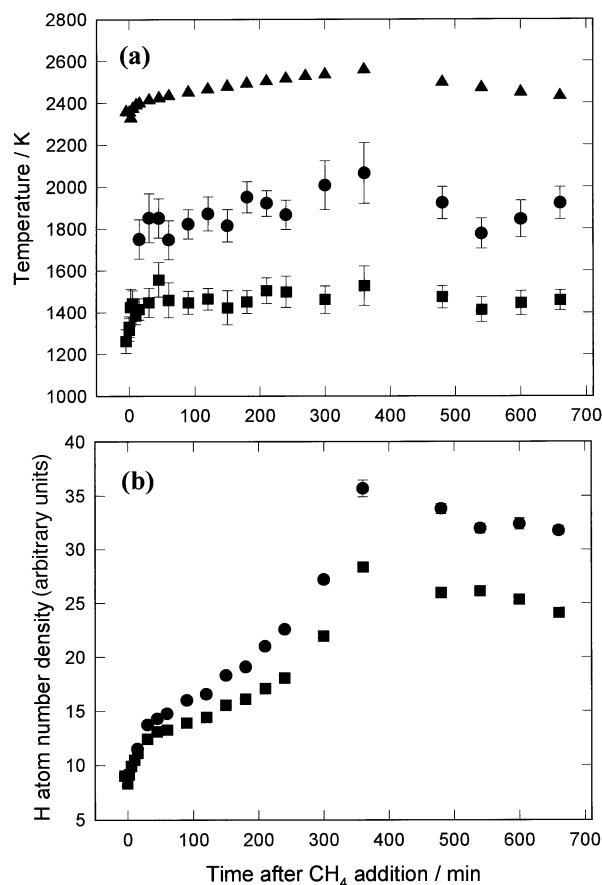


Fig. 10 H atom translational temperatures (a) and relative number densities (b) as deduced from analysis of the $2s \leftarrow 1s$ two photon Doppler lineshapes measured at $d = 0.5$ (●) and 4.5 mm (■), as a function of time after the introduction of 0.5% CH_4 to 20 Torr of H_2 . Also shown in (a) is the filament temperature measured by optical pyrometry (▲). Note that the reactor was switched off overnight, at $t = 300$ min, and restarted the next morning.

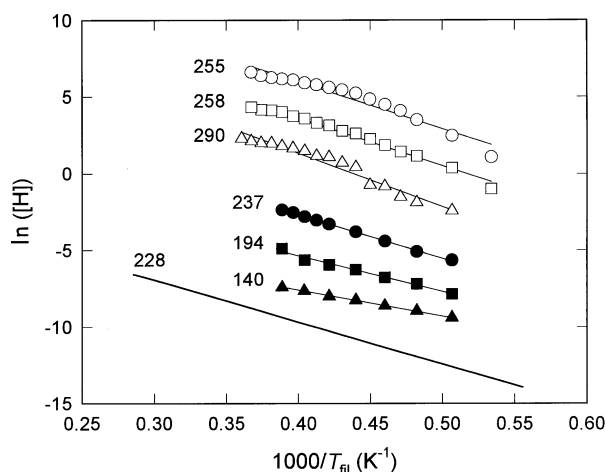


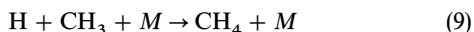
Fig. 11 Plots of $\ln[\text{H}]$ versus $1/T_{\text{fil}}$ for 20 Torr H_2 together with 0 (●), 1 (■) and 2% (▲) added CH_4 measured at $d = 1$ mm from the filament. The various data sets are offset from one another for clarity of presentation. Also shown are the measurements of Celii and Butler,⁵⁶ for the case of 0, 0.5 and 1% CH_4 in H_2 (○, □ and △, respectively). The accompanying numbers are effective ΔH_{diss} values (in kJ mol^{-1}) obtained by equating the best-fit gradients to $-\Delta H_{\text{diss}}/R$. As in Fig. 7, the bold solid line shows the dependence expected on the basis of the tabulated temperature dependence of K_f for reaction (5).

even longer time measurements would show T_{fil} settling to some rather constant, intermediary value.

Fig. 10 also illustrates the effect of CH_4 addition on $[\text{H}]$, measured at the same two radial separations from the filament. Given that a single Doppler scan takes ~ 2 min it was not possible to monitor changes in the local gas composition during the period immediately subsequent to CH_4 addition. However the early time measurements suggest that, even after 2 min, $[\text{H}]$ has started increasing. This might imply that T_{fil} was already rising during this period and that the observation of an initial apparent dip in T_{fil} is actually an artefact, reflecting some transient change in the wavelength dependence of the emissivity of the filament surface during the earliest stages of carburisation. The measured $[\text{H}]$ at $d = 4.5$ mm shows a $\sim 33\%$ rise in the first 30 min, during which time T_{fil} has risen from 2330 to 2420 K; thereafter both $[\text{H}]$ and T_{fil} rise more gradually. The observed increase in $[\text{H}]$ upon trace CH_4 additions might appear to run counter to the well documented^{5,27,71} poisoning of the catalysed dissociation of H_2 by carbon deposits on the filament surface. However, the observed increase in $[\text{H}]$ upon addition of 0.5% CH_4 is only comparable to that which would result if the same increase in T_{fil} had been applied to a pure H_2 sample [recall Fig. 6(b)]. We also note that the ratio of the H atom number densities measured in the presence of 0.5% CH_4 at $d = 0.5$ and 4.5 mm (~ 1.3 from inspection of Fig. 10) is similar to that for the corresponding d values measured in pure H_2 [Fig. 5(b)], in accord with previous suggestions²⁷ that the additional gas phase H atom loss processes, *e.g.*



and



that contribute in the presence of trace hydrocarbon additions, have little effect on the H atom radial number density profiles in a typical HFCVD reactor.

The measurements shown in Fig. 10 were obtained with a current limited power supply; increasing carburisation leads to increased filament resistance, an increase in the power supplied and thus in T_{fil} and measured $[\text{H}]$. Conversely, of course, if the power supply is voltage limited, increasing filament resistance will manifest itself as a reduction in T_{fil} . This results in a very noticeable drop in $[\text{H}]$; the drop becomes more dramatic if some critical hydrocarbon fraction is

exceeded.^{56,72} These observations, whilst principally a reflection of the drop in T_{fil} , can also be taken as indicating a progressive loss of 'active' sites on the filament surface as the extent of carburisation increases. As Fig. 11 shows, measurements of $[\text{H}]$ versus T_{fil} in the presence of small amounts of added CH_4 also yield reasonably linear van't Hoff plots, the gradients of which are found to decrease with increasing carbon fraction.

The literature contains several other plots of $[\text{H}]$ versus T_{fil} (or $\ln[\text{H}]$ versus $1/T_{\text{fil}}$), measured using dilute CH_4 - H_2 mixtures in a HFCVD reactor. The most direct previous measurements are those of Celii and Butler,⁵⁶ who used 3 + 1 REMPI to monitor $[\text{H}]$ as a function of T_{fil} at $d = 8$ mm using 0.5% and 1% CH_4 in H_2 mixtures (also reproduced in Fig. 11), while Childs *et al.*²⁷ derived estimates of $[\text{H}]$ from VUV absorption measurements of the column densities of C atoms and CH radicals in a 1% CH_4 in H_2 mixture at $d = 3$ mm. In apparent contrast to the present work, both of these earlier data sets yield van't Hoff plots with slopes at low T_{fil} that are comparable with those found for the case of pure H_2 ; all show some curvature consistent with a decrease in effective ΔH_{diss} with increasing T_{fil} . Harris and Weiner⁷⁰ estimated H atom production rates by monitoring the temperature rise attributable to H atom recombination on a thermocouple probe situated ~ 4 mm from a W filament in a 1% CH_4 - H_2 gas mixture; the plot of $\ln[\text{H}]$ versus $1/T_{\text{fil}}$ they report is somewhat steeper than that deduced in any of the laser probing studies. Two other studies have reported measurements of $[\text{H}]$, as a function of T_{fil} , where the H atoms are detected after passage through a small orifice in a substrate upon which diamond CVD is occurring. The data of Hsu *et al.*⁷² give an effective ΔH_{diss} value ($\sim 186 \text{ kJ mol}^{-1}$) comparable to that found here, while the more recent study by Zumbach *et al.*¹³ yields a curved van't Hoff plot, the mean gradient of which corresponds to a considerably lower number. Clearly, studies involving hydrocarbon addition have yielded a wide range of van't Hoff type plots, the apparent simplicity of each of which hides a multitude of complexity and will be sensitive to the prior history of the hot filament, the detailed composition of its surface and the surface temperature, and the position (relative to the filament) where the gas phase composition is probed. The steady state $[\text{H}]$ is known to be much reduced in the immediate vicinity of a heated CVD diamond surface,^{5,43,60} mainly because of H atom loss through surface abstraction reactions. $[\text{H}]$ depends on the substrate surface temperature (which is itself affected by direct heating from the hot filament), and by the local H atom flux and the extent of H atom recombination at the surface (which liberates energy to the surface). Given these additional complications, it is clear that the interpretation of $[\text{H}]$ versus T_{fil} measurements made at, or through, the substrate surface simply in terms of dissociation on the filament surface is fraught with potential ambiguity.

Conclusions

This report demonstrates the applicability of 2 + 1 REMPI spectroscopy, and subsequent analysis of the Doppler broadened lineshapes so obtained, as a means of determining relative H atom number densities and local gas temperature profiles in a purpose designed HFCVD reactor. The variation of both $[\text{H}]$ and the gas temperature with increasing filament-probe separation, d , has been investigated as a function of T_{fil} , and of H_2 pressure and flow rate, both for the case of pure H_2 and in the presence of added CH_4 . The measured trends complement and extend previous results obtained using alternative detection methods such as TALIF, *in situ* THG and/or molecular beam mass spectrometry, and are compatible with current models of the gas phase chemistry prevailing in typical HFCVD reactors. At typical process pressures (~ 20 Torr),

[H] is shown to be independent of $p(\text{H}_2)$ and to decline with increasing d in a manner consistent with diffusion from the hot filament to the walls with only minimal loss by homogeneous gas phase recombination. Measurements of the way in which [H] near the filament varies with increasing T_{fil} in 20 Torr of pure H_2 are fully consistent with dissociation on the hot filament surface being the principal route for forming H atoms; plotting $\ln[\text{H}]$ versus $1/T_{\text{fil}}$ yields a dissociation enthalpy for H atom formation, ΔH_{diss} ($\sim 237 \text{ kJ mol}^{-1}$), in good accord with the gas phase value. Similar measurements in the case of $\text{CH}_4\text{-H}_2$ mixtures also yield reasonably linear van't Hoff type plots, the gradients of which are seen to decrease as the hydrocarbon mole fraction is increased. Such observations, which reinforce some but contradict other previously reported data sets, serve to highlight some of the remaining uncertainties in modelling the diamond growth process in HFCVD reactors. Experimental studies and modelling of spatially localised measurements of [H] and the gas temperature in this reactor, in the vicinity of a diamond substrate, and their variation with distance and surface temperature, will be described elsewhere.

Acknowledgements

We are grateful to EPSRC for equipment grants and for the award of a Senior Research Fellowship (MNRA) and studentship (SAR), and to Drs J. E. Butler (Naval Research Laboratory, Washington, D.C.), S. H. Ashworth, S. R. Langford, P. W. May, A. J. Orr-Ewing and C. M. Western, and J. A. Smith and M. A. Cook, for their help and interest in aspects of this work.

References

- 1 *The Properties of Natural and Synthetic Diamond*, ed. J. E. Field, Academic Press, London, 1992.
- 2 F. G. Celii and J. E. Butler, *Ann. Rev. Phys. Chem.*, 1991, **42**, 643.
- 3 P. K. Bachmann, D. Leers and H. Lydtin, *Diamond Rel. Mater.*, 1991, **1**, 1.
- 4 M. N. R. Ashfold, P. W. May, C. A. Rego and N. M. Everitt, *Chem. Soc. Rev.*, 1994, **23**, 21.
- 5 D. G. Goodwin and J. E. Butler, in *Handbook of Industrial Diamonds and Diamond Films*, ed. M. A. Prelas, G. Popovici and L. K. Bigelow, Marcel Dekker, New York, 1988, pp. 527–81.
- 6 P. W. May, N. M. Everitt, C. G. Trevor, M. N. R. Ashfold and K. N. Rosser, *Appl. Surf. Sci.*, 1993, **68**, 299.
- 7 W. L. Hsu, *J. Appl. Phys.*, 1992, **72**, 3102.
- 8 J. A. Mucha, D. L. Flamm and D. E. Ibbotson, *J. Appl. Phys.*, 1989, **65**, 3448.
- 9 K. L. Menningen, M. A. Childs, L. W. Anderson and J. E. Lawler, *Rev. Sci. Instrum.*, 1996, **67**, 1546.
- 10 S. O. Hay, W. C. Roman and M. B. Colket, III, *J. Mater. Res.*, 1990, **5**, 2387.
- 11 K.-H. Chen, M.-C. Chuang, C. M. Penney and W. F. Banholzer, *J. Appl. Phys.*, 1992, **71**, 1485.
- 12 L. L. Connell, J. W. Fleming, H.-N. Chu, D. J. Vesteck Jr., E. Jensen and J. E. Butler, *J. Appl. Phys.*, 1995, **78**, 3622.
- 13 V. Zumbach, J. Schafer, J. Tobai, M. Ridder, T. Dreier, B. Ruf, F. Behrendt, O. Deutschmann and J. Warnatz, *J. Chem. Phys.*, 1997, **107**, 5918.
- 14 S. J. Harris, D. N. Belton, A. M. Weiner and S. J. Schmieg, *J. Appl. Phys.*, 1989, **66**, 5353.
- 15 W. L. Hsu and D. M. Tung, *Rev. Sci. Instrum.*, 1992, **63**, 4138.
- 16 C. A. Rego, R. S. Tsang, P. W. May, M. N. R. Ashfold and K. N. Rosser, *J. Appl. Phys.*, 1996, **79**, 7264 and references therein.
- 17 F. G. Celii, P. E. Pehrsson, H.-T. Wang and J. E. Butler, *Appl. Phys. Lett.*, 1988, **52**, 2043.
- 18 C. J. Chu, M. P. D'Evelyn, R. H. Hauge and J. L. Margrave, *J. Mater. Res.*, 1990, **5**, 2405.
- 19 L. R. Martin, *J. Appl. Phys.*, 1991, **70**, 5667.
- 20 S. S. Lee, D. W. Minsek, D. J. Vestcyk and P. Chen, *Science*, 1994, **263**, 1596.
- 21 S. J. Harris and A. M. Weiner, *Appl. Phys. Lett.*, 1988, **53**, 1605.
- 22 S. J. Harris, *Appl. Phys. Lett.*, 1990, **56**, 2298.
- 23 S. J. Harris and D. G. Goodwin, *J. Phys. Chem.*, 1993, **97**, 23.
- 24 M. A. Childs, K. L. Menningen, H. Toyoda, Y. Ueda, L. W. Anderson and J. E. Lawler, *Phys. Lett. A*, 1994, **194**, 119.
- 25 M. A. Childs, K. L. Menningen, P. Chevako, N. W. Spellmeyer, L. W. Anderson and J. E. Lawler, *Phys. Lett. A*, 1992, **171**, 87.
- 26 H. Toyoda, M. A. Childs, K. L. Menningen, L. W. Anderson and J. E. Lawler, *J. Appl. Phys.*, 1994, **75**, 3142.
- 27 M. A. Childs, K. L. Menningen, L. W. Anderson and J. E. Lawler, *J. Chem. Phys.*, 1996, **104**, 9111.
- 28 E. J. Corat and D. G. Goodwin, *J. Appl. Phys.*, 1993, **74**, 2021.
- 29 J. Heinze, N. Heberle and K. Kohse-Hoinghaus, *Chem. Phys. Lett.*, 1994, **223**, 305.
- 30 E. H. Wahl, T. G. Owano, C. H. Kruger, P. Zalicki, Y. Ma and R. N. Zare, *Diamond Relat. Mater.*, 1996, **5**, 373.
- 31 P. Zalicki, Y. Ma and R. N. Zare, *Appl. Phys. Lett.*, 1995, **67**, 144.
- 32 C. Kaminski and P. Ewart, *Appl. Phys. B*, 1995, **61**, 585.
- 33 J. Luque, W. Juchmann and J. B. Jeffries, *Appl. Optics*, 1997, **36**, 3261 and references therein.
- 34 D. S. Green, T. G. Owano, S. Williams, D. G. Goodwin, R. N. Zare and C. H. Kruger, *Science*, 1993, **259**, 1726.
- 35 T. G. Owano, C. H. Kruger, D. S. Green, S. Williams and R. N. Zare, *Diamond Relat. Mater.*, 1993, **2**, 661.
- 36 S. J. Harris and A. M. Weiner, *J. Appl. Phys.*, 1991, **70**, 1385.
- 37 D. G. Goodwin and G. G. Gavillet, *J. Appl. Phys.*, 1990, **68**, 6393.
- 38 T. DebRoy, K. Tankala, W. A. Yarborough and R. Messier, *J. Appl. Phys.*, 1990, **68**, 2424.
- 39 M. Frenklach and H. Wang, *Phys. Rev. B*, 1991, **43**, 1520.
- 40 E. Kondoh, T. Ohta, T. Mitomo and K. Ohtsuka, *Appl. Phys. Lett.*, 1991, **59**, 488.
- 41 D. S. Dandy and M. E. Coltrin, *J. Appl. Phys.*, 1994, **76**, 3102.
- 42 Y. A. Mankelevich, A. T. Rakhimov and N. V. Suetin, *Diamond Mater.*, 1996, **5**, 888.
- 43 Y. A. Mankelevich, N. V. Suetin and A. T. Rakhimov, *Diamond Relat. Mater.*, 1998, **7**, 1133.
- 44 N. Setaka, *J. Mater. Res.*, 1989, **4**, 664.
- 45 W. L. Hsu, *J. Vac. Sci. Technol. A*, 1988, **6**, 1803.
- 46 R. R. Rye, *Surf. Sci.*, 1977, **69**, 653.
- 47 A. B. King and H. Wise, *J. Phys. Chem.*, 1963, **67**, 1163.
- 48 R. K. Gould, *J. Chem. Phys.*, 1975, **63**, 1825.
- 49 J. Biener, U. A. Schubert, A. Schenk, B. Winter, C. Lutterloh and J. Kupperts, *J. Chem. Phys.*, 1993, **99**, 3125.
- 50 K. Tankala and T. DebRoy, *J. Appl. Phys.*, 1992, **72**, 712.
- 51 C. Wolden, S. Mitra and K. K. Gleason, *J. Appl. Phys.*, 1992, **72**, 3750.
- 52 L. Schafer, C.-P. Klages, U. Meier and K. Kohse-Hoinghaus, *Appl. Phys. Lett.*, 1991, **58**, 571.
- 53 U. Meier, K. Kohse-Hoinghaus, L. Schafer and C.-P. Klages, *Appl. Opt.*, 1990, **29**, 4993.
- 54 M. Chenevier, J. C. Cubertafon, A. Campargue and J. P. Booth, *Diamond Relat. Mater.*, 1994, **3**, 587.
- 55 A. D. Tserepi, J. R. Dunlop, B. L. Preppernau and T. A. Miller, *J. Appl. Phys.*, 1992, **72**, 2638.
- 56 F. G. Celii and J. E. Butler, *Appl. Phys. Lett.*, 1989, **54**, 1031.
- 57 F. G. Celii, H. R. Thorsheim, J. E. Butler, L. S. Plano and J. M. Pinneo, *J. Appl. Phys.*, 1990, **68**, 3814.
- 58 A. Giquel, M. Chenevier, Y. Breton, M. Petiau, J. P. Booth and K. Hassouni, *J. Phys. III*, 1996, **6**, 1167.
- 59 R. Quandt, X. Wang, Z. Min, H. L. Kim and R. Bersohn, *J. Phys. Chem. A*, 1998, **102**, 6063.
- 60 S. A. Redman, J. A. Smith, M. A. Cook and M. N. R. Ashfold, to be published.
- 61 P. D. Desai, T. K. Chu, H. M. James and C. Y. Ho, *J. Phys. Chem. Ref. Data*, 1984, **13**, 1078.
- 62 S. A. Redman, S. R. Langford, K. N. Rosser and M. N. R. Ashfold, *Proc. SPIE*, 1998, **3484**, 34.
- 63 P. J. H. Tjossem and T. A. Cool, *Chem. Phys. Lett.*, 1983, **100**, 479.
- 64 F. G. Celii and J. E. Butler, *J. Appl. Phys.*, 1992, **71**, 2876.
- 65 T. A. Cool, *Appl. Opt.*, 1984, **23**, 1559.
- 66 T. Otsuka, M. Ihara and H. Komiyama, *J. Appl. Phys.*, 1995, **77**, 893.
- 67 I. Langmuir, *J. Am. Chem. Soc.*, 1915, **37**, 417.
- 68 J. N. Smith and W. L. Fite, *J. Chem. Phys.*, 1962, **37**, 898.
- 69 M. W. Chase, Jr., C. A. Davies, J. R. Downey, Jr., D. J. Frurip, R. A. McDonald and A. N. Syverud, *J. Phys. Chem. Ref. Data*, 1985, **14**, Suppl. 1.
- 70 S. J. Harris and A. M. Weiner, *J. Appl. Phys.*, 1993, **74**, 1022.
- 71 W. L. Hsu, M. C. McMaster, M. E. Coltrin and D. S. Dandy, *Jpn. J. Appl. Phys.*, 1994, **33**, 2231.
- 72 M. Sommer and F. W. Smith, *J. Mater. Res.*, 1990, **5**, 2433.